Structural and vibrational properties of amorphous GeO_2: a molecular dynamics study

2008 J. Phys.: Condens. Matter 20 145215

(http://iopscience.iop.org/0953-8984/20/14/145215)

IOP Publishing Journal of Physics: Condensed Matter

J. Phys.: Condens. Matter **20** (2008) 145215 (7pp) doi:10.1088/0953-8984/20/14/145215

Structural and vibrational properties of amorphous GeO_2: a molecular dynamics study

Joaquín Peralta, Gonzalo Gutiérrez and José Rogan

Departamento de Física, Facultad de Ciencias, Universidad de Chile, Casilla 653, Santiago, Chile

E-mail: gonzalo@fisica.ciencias.uchile.cl

Received 27 September 2007, in final form 24 January 2008
Published 19 March 2008
Online at stacks.iop.org/JPhysCM/20/145215

Abstract

We studied the structural and dynamical properties of amorphous germanium oxide (GeO_2) by means of the molecular dynamics technique. The simulations were done in the microcanonical ensemble, with a system at a density of 3.7 g cm^{-3}, using a pairwise potential. The resulting neutron static structure factor is compared to experimental results. The network topology of our system is analyzed through partial pair correlations, coordination number and angle distributions. A detailed analysis of the interatomic distances reveals that in the amorphous state there is a short range order dominated by a slightly distorted $Ge(O_{1/2})_4$ tetrahedron. Beyond that, there is an intermediate range order composed of vertex-sharing tetrahedra. The vibrational properties were characterized by means of the density of states, obtained as a Fourier transform of the velocity autocorrelation function. The vibrational density of states has two bands, a low frequency one related to the inter-tetrahedron vibration and a high frequency band related to the intra-tetrahedron vibration.

(Some figures in this article are in colour only in the electronic version)

1. Introduction

The detailed study of the structural and vibrational properties of glasses is an important step in the understanding of short and medium range order, as well as the topology of the network. In this respect, amorphous GeO_2, or germania, is an ideally suited system, which, like amorphous SiO_2, is an archetypal oxide glass. Both can be described as a continuous network of $A(O_{1/2})_4$ (A = Si, Ge) apex-bridged tetrahedra joined to each other by oxygen atoms. The tetrahedra are randomly oriented, linked by their vertices with a broad distribution of A–O–A angles, resulting in a three-dimensional structure possessing a medium range order [1]. Also, when submitted to high pressure, both systems present a structural transition from a tetrahedral to an octahedral $A(O_{1/3})_6$, network, which implies a large change in density and in the short and medium range order [2]. But in contrast to amorphous silica, where such transformation occurs around 20 GPa, in amorphous germania it takes place between 5 and 9 GPa, which is more manageable in actual experiments.

Although germania is a chemical and structural analog of silica, and presents also considerable scientific as well as technological interest on its own, it has not been the subject of extensive studies. However, recently a thorough review has appeared [3] about the structural properties of amorphous, crystalline and liquid GeO_2. In the crystalline state germania has two phases: one low density phase (4.28 g cm^{-3}) with a quartz structure, where each Ge is coordinated with four oxygens, and a high density phase (6.25 g cm^{-3}) with rutile structure, where each Ge is coordinated with six oxygens, which is the stable structure at room conditions. The liquid state, on the other hand, is mainly composed of slightly distorted $Ge(O_{1/2})_4$ tetrahedra, which are linked to each other mainly through the corners, with a Ge–O–Ge angle of $\sim$130°.

The physical properties of the amorphous structure has been investigated both experimentally and theoretically, in particular the structural properties have been analysed by diffraction techniques [4] and molecular dynamics (MD) simulation [5, 6]. Whereas the short range order can be obtained by experiments and so far is rather well described,

the medium (or intermediate) range order is not easily deduced from an experimental point of view, and we need to rely on theoretical models. In this paper we focus our attention on the intermediate range order properties, particularly the vibrational properties of amorphous germania. In this respect, the main information comes from experiments [7, 8], and only a very recent *ab initio* MD simulation calculates the vibrational density of states [9–11]. However, it is important to have a reliable model to allow one to perform large scale molecular dynamics simulations of GeO_2 for different physical situations. This work points in that direction, validating the potential of Oeffner and Elliot [12] to be used in the amorphous state of germania, in particular for investigating its vibrational properties.

This paper is organized as follows. In section 2 we provide details of the MD simulation and the preparation of the amorphous state. Results for the short range order, network topology, diffraction pattern, and vibrational properties are presented in section 3. Finally, the conclusions are drawn in section 4.

2. Computational procedure

In molecular dynamics techniques a key issue is the choice of the interatomic potential. For this simulation we have adopted the potential developed by Oeffner and Elliot [12] for the crystalline phase. This potential is still simple and has been demonstrated to reproduce a number of experimental properties not only in the solid phase, but also in the liquid [5, 13] as well as in the amorphous state [6]. The potential employs pairwise additive Buckingham type interatomic terms of the form

$$V(r_{ij}) = \frac{q_i q_j}{r_{ij}} - \frac{A_{ij}}{r_{ij}^6} + B_{ij}\exp(-C_{ij}r_{ij}), \qquad (1)$$

where the terms represent Coulomb, van der Waals and repulsion energy, respectively. Here r_{ij} is the interatomic distance between atoms i and j. The effective charge q, the van der Waals coefficients A_{ij}, the softness parameter B_{ij} and the repulsive radius C_{ij}, are the energy parameters. Oeffner and Elliot presented two set of parameters, one corresponding to the so-called 'original potential', and the other one corresponding to the 'rescaled potential'. We use the latter one, because it better reproduces the vibrational properties of germania. The long range Coulomb interactions are calculated with the standard Ewald summation technique. The equations of motion are integrated with a modification of the Beeman algorithm, as is implemented in the program MOLDY [14], with a time step of $\Delta t = 1 \times 10^{-15}$ s.

Molecular dynamics simulations are carried out in the microcanonical ensemble (NVE) for (192Ge + 384O) units, in a cubic cell system prepared at the experimental mass density [15] $\rho = 3.7$ g cm^{-3}, using periodic boundary conditions. The amorphous state system was prepared by starting at the temperature 5000 K, with a cubic lattice which corresponds to an artificial cristobalite structure with a density of 2.9 g cm^{-3} in order to have a liquid at 5000 K at zero pressure [13]. Then, the sample is cooled to 3000 K by using a velocity scaling procedure at a rate of 0.02 K/Δt.[1] Next, the system is allowed to reach equilibrium for over 50 000Δt. With this well-equilibrated GeO_2 liquid at 3000 K we prepare our system at a density of $\rho = 3.7$ g cm^{-3}, by reducing simultaneously the lengths of the MD cell and the positions of all the atoms, in seven steps, from the initial low density of 2.9 g cm^{-3} to the final at 3.7 g cm^{-3}, having in between systems at 3.16, 3.22, 3.31, 3.40, 3.50 and 3.60 g cm^{-3}. After each shrink of the simulation cell, we thermalized the system at 3000 K for over 50 000Δt. Then, we lowered the temperature to 1500 K at a rate of 0.0075 K/Δt, and ran the system for over 50 000 time steps with temperature control, and others 50 000 steps without any disturbance. Finally, using a cooling rate of 0.0024 K/Δt, the system at 300 K was obtained. Then it was kept at constant temperature for 75 000Δt and ran another 75 000 steps without any temperature control. A summary of this schedule is showed in figure 1.

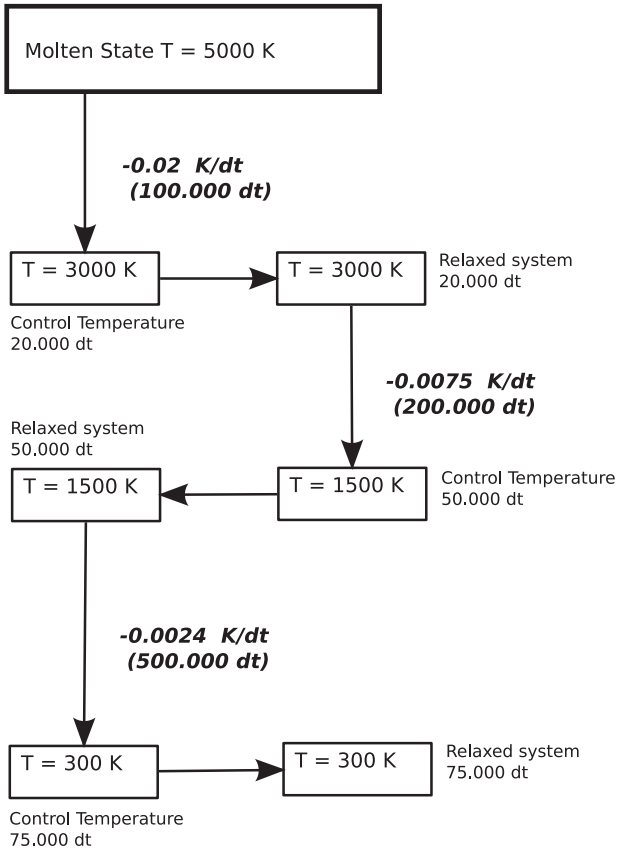

Figure 1. Schematic diagram of the quenching and thermalization schedule for preparing the amorphous GeO_2 from a well-thermalized molten state.

3. Results

The structural properties and topology of our model are inferred by means of the pair distribution functions $g_{\alpha\beta}(r)$,

[1] The cooling rate is performed by a linear scaling of the velocity, every ten time steps. To do this, we introduce a modification to the MOLDY program, which can be obtained as a patch from http://www.gnm.cl/software/thirds/parches-moldy.html.

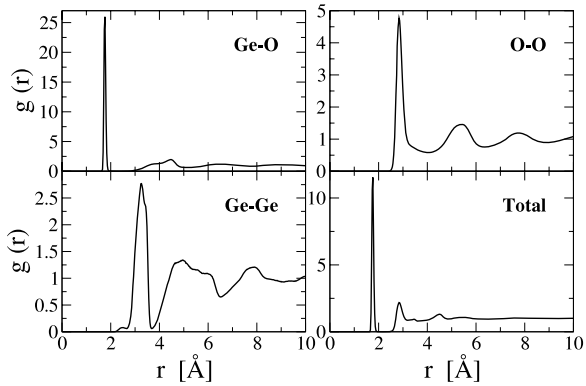

Figure 2. Partial and total pair distribution functions for amorphous GeO_2.

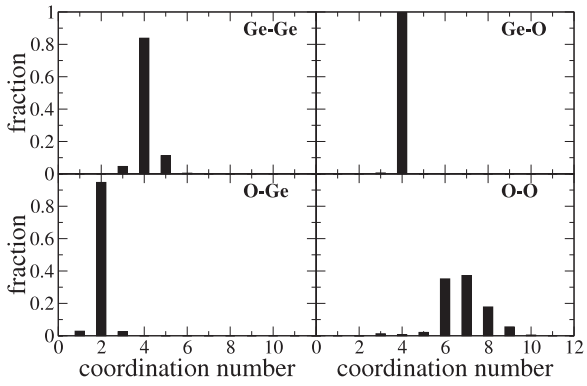

Figure 3. Distribution of Ge and O nearest neighbor coordination for amorphous GeO_2.

coordination numbers and angular distribution. Also, we compare the calculated scattering static structure factor with the experimental one. Regarding dynamical properties, we evaluated the partial and total vibrational density of states (VDOS), and compare it with the experimental data.

3.1. Structural properties

In order to assess the reliability of our computational model, we calculate the structural properties and compared them to both experimental results and previous molecular dynamics simulation. Atomic correlations are investigated by both the partial and total pair distribution functions, which are shown in figure 2. The Ge–O bond length is determined by the sharp peak observed at $R_{\mathrm{GeO}} = 1.75$ Å. The experimental result [4, 16, 17] is $R_{\mathrm{GeO}} = 1.73 \pm 0.03$ Å and the previous MD simulation [6, 18] found $R_{\mathrm{GeO}} = 1.72$ Å. The second oxygen nearest neighbors (NN) of Ge are around the distance of 4.5 Å, after a spherical shell of radius 1 Å without any oxygen atom. The nearest neighbor distance for O–O peaks at 2.84 Å and for Ge–Ge at 3.26 Å. The corresponding experimental results [4, 16] are 2.83±0.05 Å and 3.16±0.03 Å respectively. Notice that the Ge–O, O–O and Ge–Ge NN distances are all greater than silica.

The integration around the first peak in the partial pair distribution function provides the average coordination number $n_{\alpha\beta}(R) = 4\pi\rho_\beta \int_0^R g_{\alpha\beta}(r) r^2 \, \mathrm{d}r$, where R is a cut-off, usually chosen as the position of the minimum after the first peak of $g_{\alpha\beta}(r)$, corresponding in our case to 3.6, 1.9 and 3.2 Å for Ge–Ge, Ge–O and O–O distances, respectively. Average coordination numbers are 4.0 for Ge–O, 2.0 for O–Ge, 4.1 for Ge–Ge and 6.8 for O–O. A detailed description of the coordination number is provided by figure 3, which shows a histogram of Ge and O nearest neighbor coordination numbers. The Ge–O bond has a peak at 4, Ge–Ge atoms have a peak at 4, but also presents some Ge atoms that have three and five nearest neighbors. Oxygen is coordinated with two Ge atoms, while O–O coordination numbers range mainly from 6 to 9, reaching a maximum at 7. In contrast, for crystalline germania, which correspond to the rutile phase at ambient temperature and pressure, Ge are sixfold coordinated, whereas O has three Ge atoms as nearest neighbors.

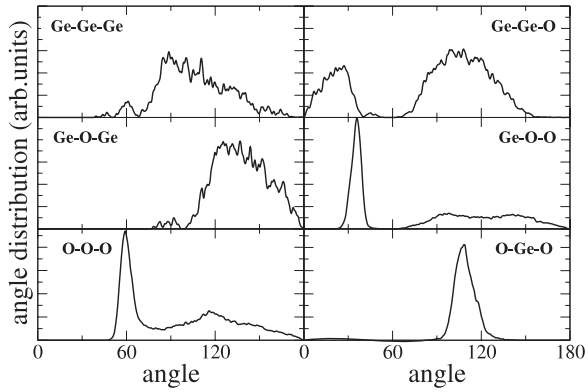

Figure 4. Distribution of bond angles for amorphous GeO_2.

Further information about the local structural units is provided by the angular distribution. In figure 4 we display the angular distribution. There is a short range order defined by a basic tetrahedron GeO_4, which is characterized by the angle O–Ge–O, with a clear peak at 109°, and the angle O–O–O, with a main peak at 60°.

These basic tetrahedra are mainly linked to each other through the vertex, forming a broad angular distribution Ge–O–Ge, centered approximately at 130°, close to the experimental value of 130° reported in [15]. This distribution also presents a small peak at around 90°, which corresponds to an edge-sharing tetrahedra forming a few twofold rings. Interestingly, our simulation is able to reproduce the experimental value of the Ge–O–Ge angle, in contrast to the MD simulation of [6], where is centered at ∼159°.

In table 1 we present a summary of our findings regarding structural properties, together with experimental and molecular dynamics simulations results. Notice that our results are closer to the *ab initio* MD results of Giacomazzi *et al* [10] than to the ones of Micoulaut *et al* [6], in spite of the latter authors used the same potential as in the present work. However, the preparation method of the amorphous sample is different and this could be the reason for the discrepancy. In this sense, it is well-known that in some cases not only the macroscopic but also the microscopic properties depend on the cooling rate [19].

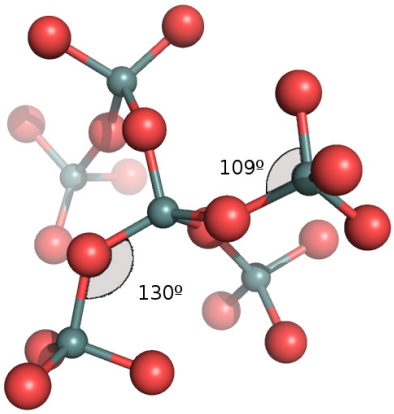

Figure 5. A typical representative polyhedron found in the simulation model of amorphous GeO_2. The tetrahedron is the building block unit of the network, which is, in general, surrounded by four tetrahedra, linked by the vertex. The small spheres correspond to germanium atoms and the big spheres to oxygen atoms.

Table 1. Interatomic distances obtained from the first peak in the measured and simulated pair distribution functions $g_{\alpha\beta}$ for amorphous GeO_2. The coordination number $n_{\alpha\beta}$ and bond angles were calculated using a cut-off value equal to the minimum after the first main peak (see details in the text). All results are from MD simulations, except [4], which corresponds to experimental data.

Pair $\alpha\beta$	$R_{\alpha\beta}$ (Å)	$n_{\alpha\beta}$	Reference
Ge–O	1.75	4.0	Present work
	1.73	3.8	[4]
	1.72	4.1	[6]
	1.78	4.01	[10]
Ge–Ge	3.26	4.1	Present work
	3.16	4.1	[4]
	3.32	4.4	[6]
	3.25	4.1	[10]
O–O	2.84	6.8	Present work
	2.83	6.7	[4]
	2.81	8.2	[6]
	2.88	7.8	[10]
Angles		(deg)	
Ge–O–Ge		130	Present work
		132	[4]
		159	[6]
		135	[10]
O–Ge–O		108.7	Present work
		≃109	[4]
		108	[6]
		≃109	[10]

Figure 5 shows a typical structure found in the simulation box. As in the case of silica glass, here also there is a short range order defined by a basic tetrahedron, and beyond that there is an intermediate range order, composed of a tetrahedron at the center, surrounded by four tetrahedra, linked by the vertex, each of them forming an angle Ge–O–Ge of approximately 130°.

In order to compare our model with the experimental results, we calculate the Fourier transform of the partial pair distribution functions, which gives the scattering static structure factor and if adequately weighted by neutron and/or x-ray factors can be compared directly to the experiments. The partial static structure factors $S_{\alpha\beta}(q)$ are given by

$$S_{\alpha\beta}(q) = \delta_{\alpha\beta} + 4\pi\rho(c_\alpha c_\beta)^{1/2} \times \int_0^R r^2\,[g_{\alpha\beta}(r) - 1]\frac{\sin(qr)}{qr}\,\frac{\sin(\pi r/R)}{\pi r/R}\,\mathrm{d}r, \qquad (2)$$

where $c_{\alpha(\beta)} = N_{\alpha(\beta)}/N$ is the concentration of $\alpha(\beta)$ species. The window function $\frac{\sin(\pi r/R)}{\pi r/R}$ has been introduced to reduce the termination effects resulting from the finite upper limit [20]. The cut-off length, R, is chosen to be half the length of the simulation box.

From here we calculate the total scattering static structure factor as $S_t(q) = \sum_{\alpha\beta}(c_\alpha c_\beta)^{1/2} S_{\alpha\beta}(q)$ and the neutron scattering static structure factor

$$S_N(q) = \frac{\sum_{\alpha\beta} b_\alpha b_\beta\,(c_\alpha c_\beta)^{1/2}[S_{\alpha\beta}(q) - \delta_{\alpha\beta} + (c_\alpha c_\beta)^{1/2}]}{\left(\sum_\alpha b_\alpha c_\alpha\right)^2}, \qquad (3)$$

where b_α denotes the coherent neutron scattering length of species α. We use $b_{\mathrm{Ge}} = 0.8193 \times 10^{-4}$ Å and $b_{\mathrm{O}} = 0.5805 \times 10^{-4}$ Å [21]. In a similar way, the x-ray diffraction factor is calculated by the formula

$$S_X(q) = \frac{\sum_{\alpha\beta} f_\alpha(q) f_\beta(q)\,(c_\alpha c_\beta)^{1/2}\,S_{\alpha\beta}(q)}{\sum_\alpha f_\alpha^2(q) c_\alpha}, \qquad (4)$$

where $f_\alpha(q)$ is the q-dependent x-ray form factor, given by $f_\alpha(q) = \sum_{i=1}^4 a_{\alpha,i}\exp[-b_{\alpha,i}(q/4\pi)^2] + c_\alpha$. The parameters $a_{\alpha,i}$, $b_{\alpha,i}$ and c_α are taken from [22] for germanium and [23] for oxygen.

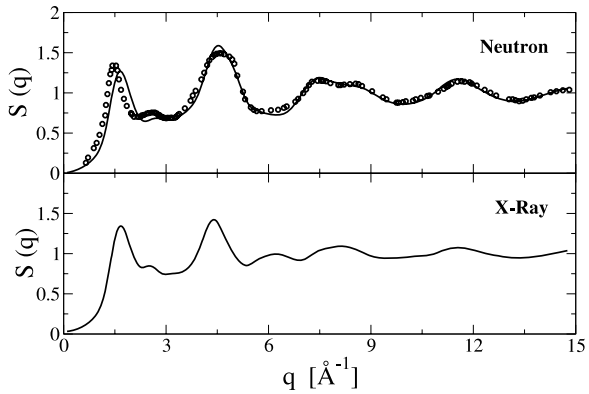

Figure 6. Neutron and x-ray structure factors for amorphous GeO_2. Dots indicate experimental results [24] and the full line our MD simulation.

Figure 6 shows the neutron and the x-ray structure factors $S(q)$ for amorphous GeO_2. It can be seen that the agreement of the calculated and experimental neutron $S(q)$ is quite good, being a small difference at the first peak, whereas the calculated one is slightly shifted to the right. In both figures, corresponding to $S_N(q)$ and $S_X(q)$, for $q \leqslant 5$ Å^{-1} three main peaks are observed, the first one at $q \sim 1.65$ Å^{-1}, a second one at $q \sim 2.7$ Å^{-1} and a third one at $q \sim 4.5$ Å^{-1}. The second peak has a rather small intensity in comparison to the

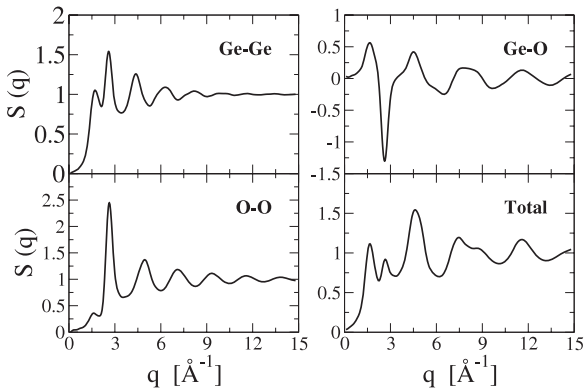

Figure 7. Partial and total scattering static structure factors for amorphous GeO_2.

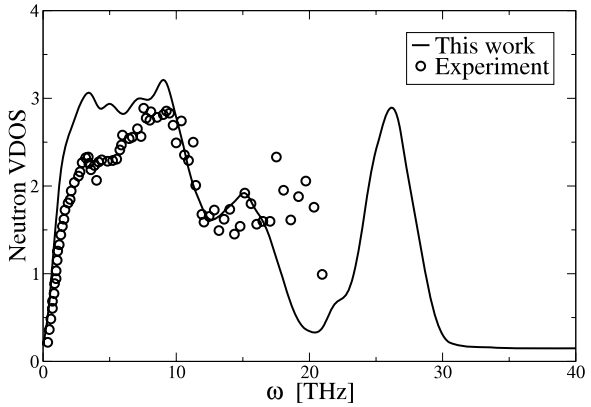

Figure 8. Neutron vibrational density of state for amorphous GeO_2 obtained from MD simulation (solid line) compared with experimental results (open circles) [8].

others two peaks. It is interesting to compare these values with the experimental ones: Sampath *et al* [24] report the first and the second peak at ∼1.6 Å^{-1} and ∼2.5 Å^{-1}, whereas the very recent work of Salmon *et al* [4] reports these peaks at ∼1.53 Å^{-1} and at ∼2.66 Å^{-1}, respectively. On the other hand, according to the molecular dynamics simulation of Micoulaut *et al* [6], the first peak is around 1.5 Å^{-1} and the second one at ∼2.5 Å^{-1}. The reason for the differences between their results and the ones of the present work should be again found in the preparation method of the amorphous state.

The origin of the peaks can be inferred by means of the partials $S_{\alpha,\beta}(q)$, which are displayed in figure 7. In fact, the first peak is due mainly to Ge–Ge correlation but also has a contribution from the Ge–O and O–O correlations, whereas the second peak has its origin in the Ge–Ge and O–O correlation and the partial cancelation due to Ge–O anti-correlation. Finally the third peak is due to all the three correlations. Notice that the large negative intensities of the $S_{\mathrm{GeO}}(q)$ between $2 < q < 4$ Å^{-1} appear because, although GeO_2 is a covalent glass, there is also present some ionic character and, thus, there are charge-transfer effects. From the structure factor, useful information can be extracted about real space correlations [25]. In analogy to the case of silica [26], we can associate the third peak (which is the highest peak) to the short range order in real space expressed in the $Ge(O_{1/2})_4$ tetrahedron. The second peak, at $q \sim 2.5$ Å^{-1} corresponds to real space correlation of $2\pi/q \simeq 2.51$ Å. The peak at lower q could be responsible for the real space correlation beyond ∼4 Å. In fact, this first peak corresponds to the so-called first sharp diffraction peak (FSDP), and from its position $q_{\mathrm{FSDP}} \sim 1.65$ Å^{-1} it can be deduced that the intermediate range order has a periodicity in real space of $2\pi/q_{\mathrm{FSDP}} \simeq 3.8$ Å. Therefore, this first peak can be associated with an intermediate range order, that is the way in which the tetrahedra are distributed, as shown in figure 5.

3.2. Vibrational properties

Dynamical properties are studied by means of the vibrational density of states $\mathcal{D}(\omega)$. We obtain $\mathcal{D}(\omega)$, calculating first the velocity autocorrelation function for species $\alpha(\beta)$,

$$Z_{\alpha(\beta)}(t) = \left\langle \sum_{i=1}^{N} m_{i\alpha} \vec{v}_{i\alpha}(0) \cdot \vec{v}_{i\alpha}(t) \right\rangle, \tag{5}$$

where $m_{i\alpha(\beta)}$ is the mass of the atom i and species $\alpha(\beta)$, $\vec{v}_{i\alpha(\beta)}$ is its velocity and $\langle \cdots \rangle$ means an average over the configurations. By performing a Fourier transform,

$$\mathcal{D}_{\alpha(\beta)}(\omega) = \frac{1}{\sqrt{2\pi}} \int \frac{Z_{\alpha(\beta)}(t)}{Z_{\alpha(\beta)}(0)} \exp(-\mathrm{i}\omega t)\, \mathrm{d}t, \tag{6}$$

the partial $\mathcal{D}_{\alpha(\beta)}(\omega)$ is obtained. From this, we obtain the total density of states, $\mathcal{D}(\omega) = \sum_\alpha c_\alpha \mathcal{D}_\alpha(\omega)$ and the total neutron section-weighted one phonon density of states [27],

$$\mathcal{D}_N(\omega) = \sum_\alpha \frac{c_\alpha 4\pi b_\alpha^2}{m_\alpha} \mathcal{D}_\alpha(\omega). \tag{7}$$

Figure 8 shows a comparison of the calculated total neutron vibrational density of states with respect to the experimental one [8]. We can see that the theoretical $\mathcal{D}(\omega)$ is slightly shifted to low frequencies with respect to the experimental $\mathcal{D}(\omega)$. (Notice, in passing, that the simulation results of the present work have had better agreement with the experimental results in the structural properties than in the vibrational spectra, a trend also present in the work of Giacomazzi *et al* [9].) In the calculated neutron $\mathcal{D}(\omega)$ can be distinguished two main bands, a lower bands up to 20 THz and a higher band from 20 to 30 THz. The partial and total vibrational density of states is shown in figure 9. The partial density of states gives the participation ratio of each species to the total density of states. It can be seen that the main contribution of the Ge vibration is at low frequency, in particular for $\omega < 5$ THz. On the other hand, the main contribution of the vibration of O atoms is at high frequency, above 20 THz. This picture is consistent with the description given by Bell [28] for SiO_2 and confirmed recently for GeO_2 by Giacomazzi *et al* [9, 11], where the lower band is related to bond-bending modes and the high band is related to the bond-stretching modes. In fact, the main contribution to the

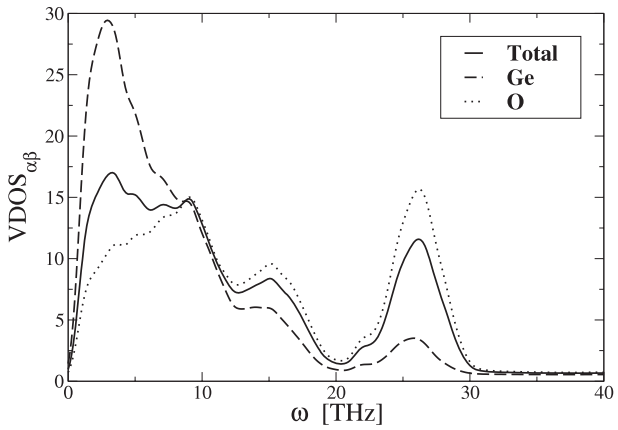

Figure 9. Total and partial vibrational density of states for amorphous GeO_2.

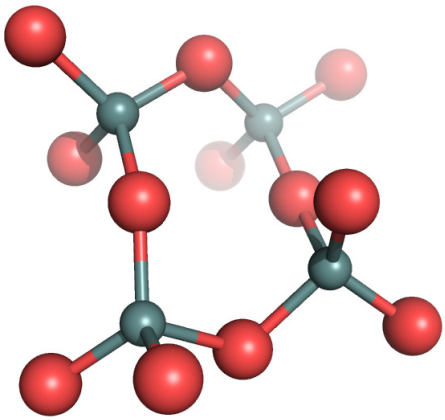

Figure 10. A typical representative structure beyond ∼4 Å found in the simulation model of amorphous GeO_2. A fourfold ring can be seen here. The small spheres correspond to germanium atoms and the big spheres to oxygen atoms.

bond-bending modes comes from Ge atoms and is associated with inter-tetrahedra vibrations, such as produced by the ring structure displayed in figure 10, whereas the bond-stretching modes are mainly due to O atoms and are associated with intra-tetrahedra vibrations.

4. Conclusion

In summary, we have presented a computer model of amorphous GeO_2, based on an empirical pairwise interatomic potential and compared it to both experimental data and previous MD simulations. According to this model, there exists a short range order, defined by the nearest neighborhood of a Ge atom, which consists of a $Ge(O_{1/2})_4$ tetrahedron, with a Ge–O bond length of 1.73 Å, longer than the Si–O bond length (1.62 Å). Beyond this basic unit, the tetrahedra are linked to each other by their vertices, forming an angle Ge–O–Ge of ∼130°, but randomly distributed in the space. Note that a-SiO_2 has a similar structure, but the Si–O–Si angle is about 142°. The dynamical properties are characterized by two main forms of vibration: bending and stretching, the former related to the inter-tetrahedron vibration and the latter related to the intra-tetrahedron vibration. This property is reflected in the VDOS in two bands. The same trend is observed in a-SiO_2, but the difference is that, whereas in a-GeO_2 the lower band goes from 0 to 20 THz and the higher band from 20 to 30 THz, in a-SiO_2 these bands go from 0 to 28 THz and from 28 to 40 THz, respectively. This shift to lower frequencies in a-GeO_2 can be explained by the increased metallicity of germanium relative to silicon, which causes a weaker Ge–O bond and a longer bond length. Interestingly, the existence of the amorphous silica-like form of carbon dioxide, a-CO_2, was recently confirmed. It could only be synthesized at high pressure [29] and, in fact, the VDOS shifted to high frequency corresponds to a-CO_2, which is supposed to be the hardest dioxide glass of group IV, a-GeO_2 being the softest. In this way, in addition to the archetypical silica and germania group IV dioxide glasses, we must now include amorphous CO_2 or carbonia. This reinforces the importance of a detailed description of each group IV dioxide glass, in order to study their similarities and differences.

Acknowledgments

This work is supported by Project PBCT Anillo ACT/24 *Computer Simulation Lab of nanobio systems* and by FONDECYT (Chile) under Grant Nos 1030063, 1070080 and 1071062. JP acknowledge a PhD fellowship from Mecesup-UCH008.

References

[1] Kohara S and Suzuya K 2005 *J. Phys.: Condens. Matter.* **17** S77–86
[2] Smith K H, Shero E, Chizmeshya A and Wolf G H 1995 *J. Chem. Phys.* **102** 6851–7
[3] Micoulaut M, Cormier L and Henderson G S 2006 *J. Phys.: Condens. Matter.* **18** R753–84
[4] Salmon P, Barnes A, Martin R and Cuello G 2007 *J. Phys.: Condens. Matter.* **19** 415110
[5] Shanavas K V, Garg N and Sharma S M 2006 *Phys. Rev.* B **73** 094120
[6] Micoulaut M, Guissani Y and Guillot B 2006 *Phys. Rev.* E **73** 031504
[7] Galeener F L, Leadbetter A and Stringfellow M 1983 *Phys. Rev.* B **27** 1052–78
[8] Pilla O, Fontana A, Caponi S, Rossi F, Viliani G, Gonzalez M, Fabiani E and Varsamis C 2003 *J. Non-Cryst. Solids* **322** 53–7
[9] Giacomazzi L, Umari P and Pasquarello A 2005 *Phys. Rev. Lett.* **95** 075505
[10] Giacomazzi L and Pasquarello A 2006 *Phys. Rev.* B **74** 155208
[11] Giacomazzi L and Pasquarello A 2007 *J. Phys.: Condens. Matter.* **19** 415112
[12] Oeffner R and Elliott S R 1998 *Phys. Rev.* B **58** 14791–803
[13] Gutiérrez G and Rogan J 2004 *Phys. Rev.* E **69** 031201
[14] Refson K 2000 *Comput. Phys. Commun.* **126** 309–29
[15] Tsiok O B, Brazhkin V V, Lyapin A G and Khvostantsev L G 1998 *Phys. Rev. Lett.* **80** 999–1002
[16] Price D L and Marie-Louise Saboungi A C B 1998 *Phys. Rev. Lett.* **81** 3207–10
[17] Stone C E, Hannon A C, Ishihara T, Kitamura N, Shirakawa Y, Sinclair R N, Umesaki N and Wright A C 2001 *J. Non-Cryst. Solids* **293–295** 769–75

[18] Micoulaut M 2004 *J. Phys.: Condens. Matter.* **16** L131–8
[19] See, for example, the study of Vollmayr K, Kob W and Binder K 1996 *Phys. Rev.* B **54** 15808
[20] Lorch E 1969 *J. Phys. C: Solid State Phys.* **C2** 229–37
[21] Koester L, Rauch H, Herkens M and Schröder K 1981 Summary of neutron scattering lengths *KFA Report* Jül–1755 1755
[22] Cromer D T and Weber J T 1974 *International Tables for X-Ray Crystallography* vol IV, ed J A Ibers and W C Hamilton (Birmingham: Kynoch Press) chapter 2.2, p 71
[23] Tokonami M 1965 *Acta Crystallogr.* **19** 486
[24] Sampath S, Benmore C, Lantzky K, Neuefeind J, Leinenweber K, Price D and Yarger J 2003 *Phys. Rev. Lett.* **90** 115502
[25] Salmon P S 1994 *Proc. R. Soc.* A **445** 351
[26] Vashishta P, Kalia R K, Rino J P and Ebbsjö I 1990 *Phys. Rev.* B **41** 12197–209
[27] Loong C, Vashishta P, Kalia R and Ebbsjo I 1995 *Europhys. Lett.* **31** 201–6
[28] Bell R J 1972 *Rep. Prog. Phys.* **35** 1315–409
[29] Santoro M, Gorelli J A, Bini R, Ruocco G, Scandolo S and Crichton W A 2006 *Nature* **441** 857–60